

# On-device Sora: Enabling Diffusion-Based Text-to-Video Generation for Mobile Devices

Bosung Kim

Ulsan National Institute of Science  
and Technology  
South Korea  
bosung.k@unist.ac.kr

Kyuhwan Lee

Ulsan National Institute of Science  
and Technology  
South Korea  
hanbitchan@unist.ac.kr

Isu Jeong

Ulsan National Institute of Science  
and Technology  
South Korea  
ijeong@unist.ac.kr

Jungmin Cheon

Ulsan National Institute of Science  
and Technology  
South Korea  
jungmin0210@unist.ac.kr

Yejin Lee

Ulsan National Institute of Science  
and Technology  
South Korea  
yeojin@unist.ac.kr

Seulki Lee

Ulsan National Institute of Science  
and Technology  
South Korea  
seulki.lee@unist.ac.kr

## Abstract

We present On-device Sora, a first pioneering solution for diffusion-based on-device text-to-video generation that operates efficiently on smartphone-grade devices. Building on Open-Sora, On-device Sora applies three novel techniques to address the challenges of diffusion-based text-to-video generation on computation- and memory-limited mobile devices. First, Linear Proportional Leap (LPL) reduces the excessive denoising steps required in video diffusion through an efficient leap-based approach. Second, Temporal Dimension Token Merging (TDTM) minimizes intensive token-processing computation in attention layers by merging consecutive tokens along the temporal dimension. Third, Concurrent Inference with Dynamic Loading (CI-DL) dynamically partitions large models into smaller blocks and loads them into memory for concurrent model inference, effectively addressing the challenges of limited device memory. We implement On-device Sora on the iPhone 15 Pro, and the experimental evaluations demonstrate that it is capable of generating high-quality videos on the device, comparable to those produced by Open-Sora running on high-end GPUs. These results show that On-device Sora enables efficient and high-quality video generation on resource-constrained mobile devices, expanding accessibility, ensuring user privacy, reducing dependence on cloud infrastructure, and lowering associated costs. We envision the proposed On-device Sora as a significant first step toward democratizing state-of-the-art generative technologies, enabling video generation capabilities on commodity mobile and embedded devices. The code implementation is publicly available at an GitHub repository<sup>1</sup>.

## 1 Introduction

Recent advancements in generative models [62] have significantly expanded capabilities in data generation across various modalities, including text [31], image [58], and video [64]. In particular, diffusion-based models for image tasks [16, 28, 50, 51, 54, 56, 60, 77] have emerged as foundational tools for a wide range of applications, such as image generation [29], image editing [34], and personalized content creation [78]. Further extending these technologies, diffusion-based generative models are now driving remarkable progress in video generation tasks [6, 7, 25, 27, 30, 35, 44, 45, 59, 68, 70], including video synthesis [39] and real-time video analysis [48], facilitating the development of advanced generative video services and applications in new and unprecedented ways.

One of the most notable video generation models is Sora [41], which has demonstrated remarkable potential in creating high-quality videos from textual descriptions (prompts), effectively transforming abstract concepts into visually realistic content. However, the inherently high complexity of diffusion processes for video generation, combined with the substantial size of diffusion-based Transformer models [50], imposes significant computational and memory demands. For instance, Sora [41] is estimated to take an hour to produce five minutes of video using an NVIDIA H100 GPU of 80 GB RAM. Compared to large language models (LLMs) [79], the costs for diffusion-based video generation models like Sora are several orders of magnitude higher, indicating their resource-intensive nature. As a result, the accessibility of video generative services remains predominantly confined to environments with extensive computational resources, limiting their applicability in resource-constrained devices.

With the rapid expansion of mobile, IoT, and embedded devices, there is a growing demand for running generative applications directly on the device. In response, numerous

<sup>1</sup><https://github.com/eai-lab/On-device-Sora>

studies have primarily focused on the development of on-device image generation [10, 13, 14, 38, 66, 80], as image generation is comparatively less resource-intensive than video. However, enabling on-device video generation remains in its nascent stages due to the significantly higher computational and memory resource demands compared to image generation [18]. Moreover, given that video data is typically much larger and more sensitive than image data [15], there is an increasing need for innovative technologies that can enable efficient and effective on-device video generation.

We introduce On-device Sora, the first standalone framework for diffusion-based on-device text-to-video generation, which is capable of producing high-quality videos on smartphone-grade devices. On-device Sora leverages Open-Sora [82] as its backbone and significantly enhances the efficiency of video generation while maintaining the comparable video quality, enabling on-device text-to-video generation with limited computational power and memory. To the best of our knowledge, On-device Sora proposed in this work is the first solution that enables the efficient generation of Sora-level video directly on the device, which has previously been restricted to large-scale data center environments.

On-device Sora addresses three fundamental challenges in enabling diffusion-based on-device text-to-video generation. First, diffusion-based video generation entails a substantial number of denoising steps, requiring repeated executions of diffusion models, ranging from dozens to thousands of iterations. To address this, we propose Linear Proportional Leap (LPL), which reduces nearly half of the denoising steps by leaping through a large portion of steps using the Euler’s method [5] in an estimated direct trajectory to generate videos efficiently. Second, state-of-the-art diffusion models, such as STDiT (Spatial-Temporal Diffusion Transformer) [82], employed by Open-Sora, exhibit high computational complexity due to their substantial amount of token processing [8] in attention modules [67]. To tackle the high computational complexity of STDiT, we propose Temporal Dimension Token Merging (TDTM), which merges consecutive tokens [8, 9] in temporal order at attention layers of STDiT, effectively reducing the token processing up to a quarter. Lastly, the substantial size of state-of-the-art models required for text-to-video generation, i.e., T5 [52] and STDiT [82], presents challenges for execution on memory-constrained mobile devices. To overcome this, we propose Conference Inference and Dynamic Loading (CI-DL), which integrates concurrent model inference with the dynamic loading of models into memory. It dynamically divides the model into blocks and loads them into memory based on the device’s available memory capacity at run-time, allowing simultaneous model block loading and inference. With these three proposed methods, high-quality video generation becomes feasible on smartphone-grade devices with

limited computing resources, overcoming the requirements for substantial computational power, such as high-end GPUs.

Currently, video generative technology remains neither widely accessible nor commonly available to the public [41]. Therefore, enabling video generation on commodity mobile and embedded devices can not only enhance the accessibility of advanced video generation technologies but also provide additional benefits. Users can ensure privacy and mitigate concerns about data transmission and leakage of sensitive personal information. On-device video generation eliminates the need for interaction with the third-party cloud servers, which may pose security risks due to potential data breaches or unauthorized access. Furthermore, cloud-based generative models often suffer from latency issues influenced by network speed and may not function optimally when connectivity is unstable or unavailable. On-device generative models, in contrast, can provide more reliable services, offering stable functionality regardless of network conditions. Another limitation of cloud-based video generation is their shared nature, which limits personalization and the ability to cater to individual users. On-device video generation, however, can be tailored to each user, enabling personalized experiences through customized video creations. Through on-device generation, videos can be fine-tuned and customized for individual users, providing contents that better reflect personal preferences, data, contexts, and environments. From a financial perspective, generating videos on-device is far more economical. For example, the cost of an NVIDIA H100 GPU is around \$25,000, whereas an iPhone 15 Pro is about only \$999, which is 25 times more affordable. Additionally, the annual maintenance costs for cloud-based video generation are estimated to range between \$250,000 and \$800,000, whereas a smartphone incurs negligible maintenance expenses.

We implement On-device Sora on the iPhone 15 Pro [2] based on Open-Sora [82], which is an open-source text-to-video generation framework, enabling standalone text-to-video generation directly on the device. The full implementation is available as open-source code in a publicly accessible anonymous GitHub repository<sup>1</sup>. The extensive experiments are conducted to evaluate the performance of the proposed On-device Sora using the state-of-the-art video benchmark tool, i.e., VBench [32], compared with Open-Sora running on NVIDIA A6000 GPUs. The experimental results demonstrate that On-device Sora can effectively generate videos of equivalent quality to Open-Sora [82], while accelerating video generation when applying the proposed three methods. While the iPhone 15 Pro has a GPU of 143 times less computational power [2] and 16 times smaller memory (RAM) compared to the NVIDIA A6000 GPU, the evaluation results demonstrate that On-device Sora significantly improves the efficiency of video generation by effectively compensating for the limited computing resources of the device.

## 2 Background and Key Challenges

We first provide 1) a background of Open-Sora [82], an open-source video diffusion model, which is the backbone of the proposed On-device Sora, and 2) key challenges in realizing on-device video generation for mobile devices.

### 2.1 Background: Open-Sora

Figure 1 illustrates the structure of Open-Sora [82], generating videos from prompts (texts) through 1) prompt embedding, 2) latent video generation, and 3) video decoding.

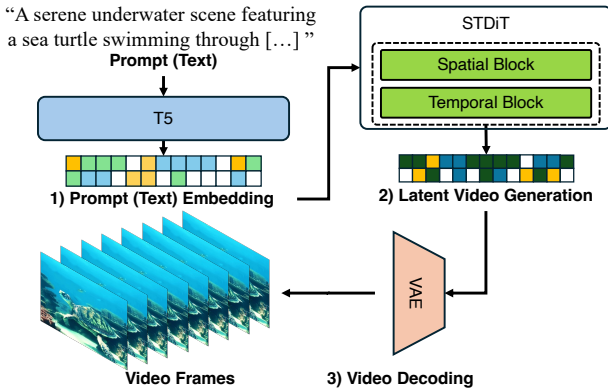


Figure 1: Open-Sora [82] generates realistic videos from the user prompt (text) through three stages: 1) prompt embedding, 2) latent video generation, and 3) video decoding.

**1) Prompt (Text) Embedding.** The first stage of Open-Sora [82] is to map a user prompt, a textual description of the desired video, to an embedding vector, which is used as input for the subsequent video generation stage. To produce prompt embeddings from user texts, Open-Sora employs T5 (Text-to-Text Transformer) [52], a language model specifically fine-tuned to support video generation tasks.

**2) Latent Video Generation.** The next stage is to generate the latent video representation conditioned on the prompt embedding obtained from T5 (Text-to-Text Transformer) [52]. To this end, Open-Sora employs STDiT (Spatial-Temporal Diffusion Transformer) [82], a diffusion-based text-to-video model using the Markov chain [76]. Since maintaining temporal consistency across video frames is essential in video generation, STDiT [82] applies the spatial-temporal attention mechanism [72] to the patch representations. It allows effective learning of temporal features across video frames through the temporal attention, enhanced by incorporating rope embeddings [61]. During the forward process of STDiT, the Gaussian noise  $\epsilon_k$  is iteratively added to the latent video representation  $\mathbf{x}_k$  over  $K$  steps, transforming the intact video representation  $\mathbf{x}_0$  into the complete Gaussian noise  $\mathbf{x}_K$  in the

latent space with the forward distribution  $q(\mathbf{x}_k|\mathbf{x}_{k-1})$  as:

$$\mathbf{x}_k = \sqrt{1 - \beta_k} \mathbf{x}_{k-1} + \sqrt{\beta_k} \epsilon_k \quad (1)$$

$$q(\mathbf{x}_t|\mathbf{x}_{k-1}) = \mathcal{N}(\mathbf{x}_t; \sqrt{1 - \beta_k} \mathbf{x}_{k-1}, \beta_k \mathbf{I})$$

where  $\beta_k$  is the parameter determining the extent of noise.

To generate (recover) the latent representation  $\mathbf{x}_0$ , the noise  $\epsilon_k$  is repeatedly removed (denoised) from the complete Gaussian noise  $\mathbf{x}_K$  through the reverse process using the estimated noise with the reverse distribution  $p_\theta(\mathbf{x}_{k-1}|\mathbf{x}_t)$  modeled by STDiT [82] with the parameter set  $\theta$ , as follows:

$$\mathbf{x}_{k-1} = \mu_\theta(\mathbf{x}_k, k) + \sqrt{\beta_k} \epsilon \quad \text{where } \epsilon \sim \mathcal{N}(\mathbf{0}, \mathbf{I}) \quad (2)$$

$$p_\theta(\mathbf{x}_{k-1}|\mathbf{x}_k) = \mathcal{N}(\mathbf{x}_{k-1}; \mu_\theta(\mathbf{x}_k, k), \Sigma_\theta(\mathbf{x}_k, k))$$

where  $\mu_\theta(\mathbf{x}_k, k)$  and  $\Sigma_\theta(\mathbf{x}_k, k)$  is the mean and variance of  $\mathbf{x}_k$  estimated by the STDiT model training, respectively. This reverse process repeatedly denoises  $\mathbf{x}_k$  into  $\mathbf{x}_{k-1}$  over a large number of  $1 \leq k \leq K$  denoising steps (i.e., from dozens to thousands of steps), eventually generating the de-noised latent video representation  $\mathbf{x}_0$  close to the intact representation.

**3) Video Decoding.** Finally, the latent video representation  $\mathbf{x}_0$  generated from STDiT is decoded and up-scaled into the human-recognizable video through the VAE (Variational Autoencoder) [17]. The VAE employed in Open-Sora utilizes both 2D and 3D structures; the 2D VAE is based on SDXL [51], while the 3D VAE adopts the architecture of Magvit-v2 [74].

### 2.2 Challenges in On-device Video Generation

Although Open-Sora [82] has enabled the generation of high-quality videos from texts, adapting this advanced generative capability to mobile devices presents key challenges.

**C1) Excessive Denoising Steps.** Table 1 shows the latency of each model component in Open-Sora, where the latent video generation process (denoising process) performed by STDiT is the most time-consuming. That is because a substantial number of denoising steps is required to remove the noise  $\epsilon_k$  from  $\mathbf{x}_K$  to obtain  $\mathbf{x}_0$  during latent video generation [60]. Such extensive denoising iterations presents considerable challenges on mobile devices with constrained computational capabilities. To reduce the number of denoising steps, Open-Sora employs Rectified Flow [40], which redefines the objective of diffusion models, inducing the model to directly approximate the straight mapping trajectory between the initial and target distributions. In image generation, it enables a single-step denoising without a significant loss in image quality. However, in video generation models [1, 82], the accumulated variance across sequential video frames prevents the trajectory from being fully represented with a single drift. As a result, Open-Sora [82] requires at least  $K = 30$  or 50 denoising steps to produce high-quality videos. While the numerous denoising steps are manageable in server-level environments—where the complete denoising

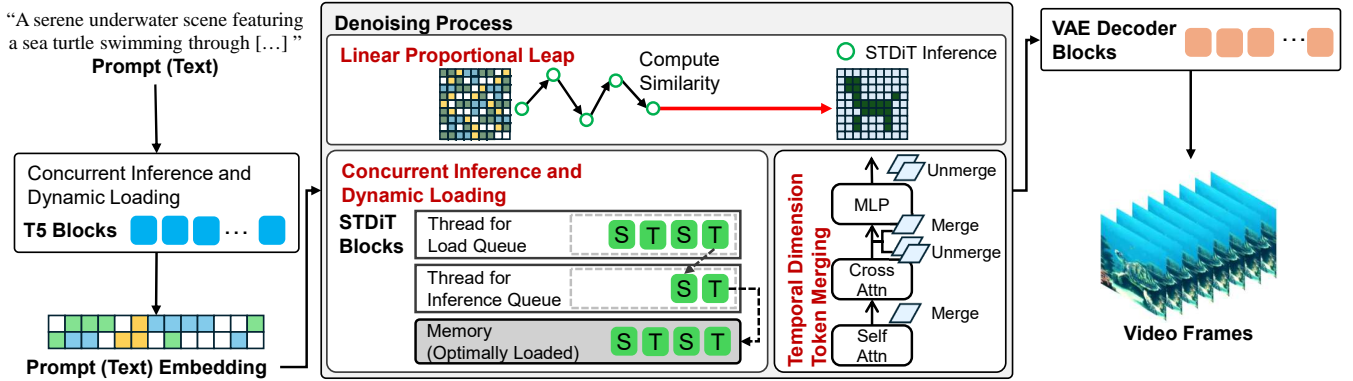


Figure 2: On-device Sora enables efficient text-to-video generation directly on the device by employing three key approaches: 1) Linear Proportional Leap, 2) Temporal Dimension Token Merging, and 3) Concurrent Inference with Dynamic Loading.

Table 1: The number of executions (iterations) of each model component (i.e., T5 [52], STDiT [82], and VAE [17]) in Open-Sora [82] and their total latencies on iPhone 15 Pro [2].

Component	Iterations	Inference Time (s)	Total Latency (s)
T5 [52]	1	110.505	110.505
STDiT [82]	50	35.366	1768.320
VAE [17]	1	135.047	135.047

process typically finishes within one minute—on mobile devices, it may take several tens of minutes for full denoising. Accordingly, a new approach to reduce denoising steps is essential to enable efficient on-device video generation.

**C2) Intensive Token Processing.** While a large number of denoising steps poses a significant challenge to video generation on mobile devices, even a single denoising step itself is computationally intensive. The primary reason is that the computational complexity of the attention mechanism [47] in STDiT [82] grows quadratically with the token size, which significantly increases the computational load for token processing and, consequently, the model’s inference latency. To address this challenge, Token merging [9] has been proposed to improve the throughput of vision Transformer models. Token merging progressively merges similar visual tokens within the transformer to accelerate the model inference latency by reducing the size of tokens to be processed. While token merging has been applied to diffusion models, it is only applied to spatial tokens [8, 9] and has not been applied to the temporal tokens in video diffusion models, such as STDiT [82]. Thus, a novel token merging method is required to improve the computational efficiency of token processing in video generation, while preserving high video quality.

**C3) High Memory Requirements.** Figure 3 shows the memory requirements of model components executed by Open-Sora [82], i.e., VAE [17], T5 [52], and STDiT [82], where their cumulative memory demand, i.e., 23 GB, can easily surpass the memory capacity of many mobile devices. For

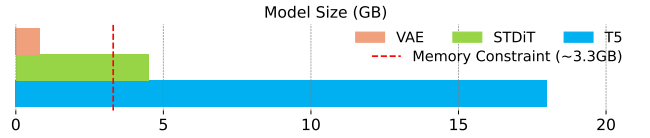


Figure 3: The size of Open-Sora models: T5 [52] (18.00 GB), STDiT [82] (4.50 GB), and VAE [17] (0.82 GB), which exceeds the available memory capacity of iPhone 15 Pro [2] (3.3 GB).

instance, the iPhone 15 Pro [2], with 8 GB of memory, restricts the available memory for a single application to 3.3 GB to ensure the system stability. Furthermore, the individual memory requirements of T5 and STDiT exceed 3.3 GB, creating challenges in loading them into memory. In addition, some memory must be reserved for model execution (inference), complicating the deployment of Open-Sora on mobile devices. Thus, executing large video generative models with limited device memory is another challenge that should be addressed to enable on-device video generation.

### 3 Overview: On-device Sora

Building on Open-Sora [82] outlined above (Sec. 2.1), we propose On-device Sora (Figure 2), which enables diffusion-based text-to-video generation on mobile devices by addressing the key challenges (Sec. 2.2), as summarized below.

**1) Linear Proportional Leap (Sec. 4).** To reduce the excessive number of denoising steps, we propose Linear Proportional Leap, which enables the generation of high-quality videos with nearly half of the required full denoising steps. This is achieved by leveraging the linear trajectory properties of Rectified Flow [40] employed in STDiT [82]. Instead of performing the full sequence of denoising steps during video generation, it makes a direct leap along the linear trajectory toward the target data at the middle of the denoising process by utilizing the pre-trained flow fields [40]. Thus,

Linear Proportional Leap effectively reduces the most time-consuming stage of video generation—the iterative execution of STDiT [82]—by minimizing the number of denoising steps. Notably, this reduction in denoising steps is accomplished without necessitating additional model training, architectural modifications, or data calibration, allowing for saving substantial time and computational resources.

**2) Temporal Dimension Token Merging (Sec. 5).** To lighten the intensive computation required for token processing, we propose Temporal Dimension Token Merging, which merges consecutive video frames in the form of latent representations at each attention layer of STDiT [82]. The proposed token merging reduces the amount of tokens to be processed by half and lowers the computational load of attention modules up to one-quarter. To the best of our knowledge, it is the first to merge tokens in temporal order at attention layers in diffusion-based video generation models.

**3) Concurrent Inference with Dynamic Loading (Sec. 6).** To execute large video generative models (i.e., T5 [52] and STDiT [82]) with the limited device memory, we propose Concurrent Inference with Dynamic Loading, which partitions the models into smaller blocks that can be loaded into the memory and executed concurrently. By parallelizing model execution and block loading, it effectively accelerates iterative model inference, e.g., multiple denoising steps. Also, it improves memory utilization while minimizing the block loading overhead by retaining specific model blocks in memory dynamically based on the available runtime memory.

## 4 Linear Proportional Leap

We reduce the excessive number of denoising steps performed by STDiT [82] by introducing Linear Proportional Leap (LPL), which leverages the trajectory characteristics of Rectified Flow [40]. It allows early stop of denoising steps through proportionally scaled linear leaps, without any extra model training or modification of the STDiT architecture.

### 4.1 Rectified Flow

The reverse diffusion process is performed through multiple denoising steps, transforming an initial Gaussian distribution into a desired distribution corresponding to the input prompt. Several ODE-based methods [43, 81] reformulate this process by training neural network models to predict the drift at each time point, building the distribution trajectories from the initial to the target point by using ODE solvers [55, 73].

Rectified Flow [40] simplifies the transition from the initial point to the target point by training the model to predict a drift aligned with the direct linear trajectory connecting these two points. Using the Euler method [12], the  $k$ th trajectory  $\mathbf{z}_k$  is derived by updating the previous trajectory  $\mathbf{z}_{k-1}$

with the estimated drift  $\mathbf{v}(P_k, t_k)$  and step size  $dt_k$  defined by two sampled time steps  $t_k$  and  $t_{k+1}$ , as follows:

$$\mathbf{z}_k = \mathbf{z}_{k-1} + \mathbf{v}(P_k, t_k)dt_k \quad \forall 1 \leq k \leq K$$

$$\text{where } t_k \in [0, 1] \text{ and } dt_k = \begin{cases} t_k - t_{k+1}, & \text{if } t_k \neq t_K \\ t_k, & \text{if } t_k = t_K. \end{cases} \quad (3)$$

Here, the time step  $t_k \in [0, 1]$  corresponds to the normalized reverse process at the  $k$ th denoising step, with  $t_k = 1$  representing the time step at which data is fully noisy (start of denoising) and  $t_k = 0$  corresponding to the time step when data reaches the desired distribution (end of denoising). The drift  $\mathbf{v}(P_k, t_k)$  is predicted from STDiT [82] given the  $k$ th position on the trajectory,  $P_k = t_k P_1 + (1 - t_k)P_0$ , computed from linear interpolation with sampled time step,  $t_k$  [40].

In Rectified Flow [40], the model is trained to predict the direct direction toward target point at any point on the trajectory. This allows diffusion-based image generation models for achieving a denoising process in few steps without significant performance degradation. While the actual trajectory may not be fully captured by a single drift, it can be effectively approximated with a reduced number of drifts. However, in diffusion-based video generation, achieving single-step generation is challenging due to the additional temporal variance of video data and the increased complexity of the target distribution. With Rectified Flow [40], Open-Sora [82] generates video outputs with  $K = 30$  or  $50$  denoising steps, in contrast to image generation, which produces images in a single step.

### 4.2 Linear Proportional Leap

Building upon Rectified Flow [40], Linear Proportional Leap reduces denoising steps, as illustrated in Figure 4.

If the  $n$ th data distribution is sufficiently close to the  $K$ th target distribution in the denoising process, the trajectories  $\mathbf{z}_{n+1\dots K}$  would be approximately straight for the remaining time steps  $t_{n+1\dots K}$ , making the estimation of the drift  $\mathbf{v}(P_k, t_k)dt_k$  in Equation (3) unnecessary for  $k > n$ . Consequently,  $\mathbf{v}(P_k, t_k)dt_k$  is estimated only for  $1 \leq k \leq n$ , allowing the denoising process to stop early at the  $(n + 1)$ th step, rather than continuing to the full  $K$ th step. For the remaining time steps  $t_{n+1\dots K}$ , the trajectories  $\mathbf{z}_{n+1\dots K}$  linearly leap towards the target data distribution, with the straight direction of  $\mathbf{v}(P_{n+1}, t_{n+1})$  and  $dt_{n+1}$  scaled proportionally to  $t_{n+1\dots K}$ .

By assuming  $k = K$ ,  $\mathbf{z}_k$  is derived from Equation (3) as:

$$\begin{aligned} \mathbf{z}_k &= \mathbf{z}_{k-1} + \mathbf{v}(P_k, t_k)dt_k \\ &= \mathbf{z}_0 + \sum_{i=1}^{k-1} \mathbf{v}(P_i, t_i)(t_i - t_{i+1}) + \mathbf{v}(P_k, t_k)t_k \end{aligned} \quad (4)$$

If the denoising process stops at the step  $n$ , the  $n$ th trajectory can be represented as  $\mathbf{z}_n = \mathbf{z}_0 + \sum_{i=1}^n \mathbf{v}(P_i, t_i)(t_i - t_{i+1})$ .



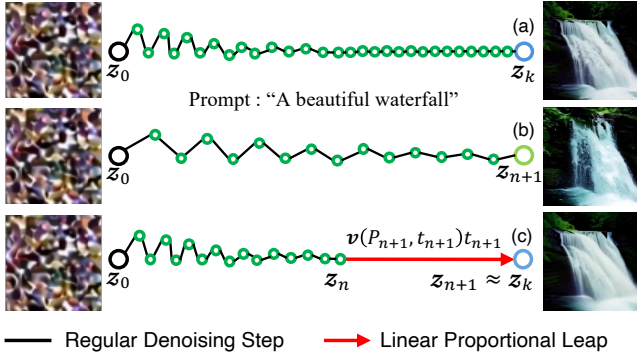


**Figure 4: An abstracted illustration of trajectories and latent visualizations for  $K = 30$  and  $n = 15$ : (a) Rectified Flow [40] with full  $k = 30$  denoising steps, generating intact and complete data, (b) Rectified Flow [40] with  $n + 1 = 16$  denoising steps without applying Linear Proportional Leap, resulting in low-quality data generation from variance with high step sizes ( $dt_k$ ), and (c) Linear Proportional Leap with  $n + 1 = 15 + 1$  denoising steps, producing data nearly equivalent to (a).**

Then, if we apply the identical drift  $\mathbf{v}(P_{n+1}, t_{n+1})dt_{n+1}$  to the remaining  $n + 1 \leq i \leq k$  steps, Equation (4) becomes:

$$\begin{aligned} \mathbf{z}_k &= \mathbf{z}_n + \mathbf{v}(P_{n+1}, t_{n+1}) \sum_{i=n+1}^{k-1} (t_i - t_{i+1}) + \mathbf{v}(P_{n+1}, t_{n+1})t_k \\ &= \mathbf{z}_n + \mathbf{v}(P_{n+1}, t_{n+1})(t_{n+1} - t_{n+2} + \dots + t_{k-1} - t_k + t_k) \\ &= \mathbf{z}_n + \mathbf{v}(P_{n+1}, t_{n+1})t_{n+1} \end{aligned} \quad (5)$$

Thus, the required denoising steps are reduced to  $n + 1$  out of the total  $k$  steps, allowing STDiT to be executed only  $n + 1$  times, with the last  $(n + 1)$ th trajectory applied to its time step  $t_{n+1}$ . Replacing  $dt_k$  with  $t_{n+1}$  in Equation (5), instead of computing difference between the sampled time steps, can invoke an identical effect under assumption that later steps tend to sustain their drift directions. It enables the immediate completion of the denoising process, as  $t_{n+1}$  is equivalent to the remaining steps required to reach the end of denoising.

For instance, when  $K = 30$  and  $n = 15$ , the denoising steps proceed for the initial  $n = 15$  steps, and at step  $n = 16$ , the trajectory transitions by leaping towards the linear direction of the target distribution. Due to the straightened trajectory, whose straightness increases as the denoising process approaches its end, combining the current drift with the product of the remaining step size yields a result that closely approximates the outcome achievable through the full denoising process. This enables a reduction of the denoising process by half without requiring additional model training.

Linear Proportional Leap can be dynamically applied by measuring the cosine similarity between two consecutive drifts  $\mathbf{v}$  at runtime. When the cosine similarity appears that the current trajectory is sufficiently linear, a linear leap is

made proportionally to the remaining steps. Figure 5 visualizes the cosine similarities between consecutive drifts, which stabilizes after a certain number of steps, suggesting that the trajectory toward the target data distribution is nearly linear. This enables fewer steps by utilizing the leap with the larger step size to efficiently progress to the desired direction.

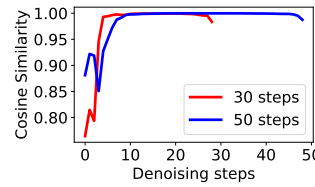


**Figure 5: An example of cosine similarities between two consecutive drifts estimated from STDiT [82], i.e.,  $\mathbf{v}(P_n, t_n)$  and  $\mathbf{v}(P_{n-1}, t_{n-1})$  for 30 (red) and 50 steps (blue).**

## 5 Temporal Dimension Token Merging

We streamline the computational complexity of the denoising process by introducing Temporal Dimension Token Merging (TDTM), which halves the size of tokens within STDiT [82] along the temporal dimension, decreasing the computation of the self-attention quadratically and the cross-attention in half. Unlike existing token merging primarily apply to self-attentions over the spatial dimension, which exhibits suboptimal performance [8, 9, 21, 37], Temporal Dimension Token Merging leverages the temporal aspect of video frames to reduce computations while ensuring the video quality.

### 5.1 Token Merging

STDiT [82] consists of multiple attention layers, i.e., cross- and self-attention, of the linear and quadratic complexity, respectively. In video generation, these attentions extend across two dimensions, i.e., spatial and temporal dimension.

General model optimization techniques, e.g., pruning [53], quantization [24], and distillation [26], may reduce the STDiT’s computational complexity. However, they often necessitate model re-training (fine-tuning) or specialized hardware for implementation, and most importantly, the performance of video generation can hardly be preserved. In contrast, token merging [9] reduces the size of tokens processed in attention layers, decreasing computational complexity without requiring model re-training or hardware-specific adaptations.

In STDiT [82], the attention bias influenced by input tokens in cross-attention layers leads to higher computational demands compared to self-attention layers. As a result, developing an effective token merging method for cross-attention is crucial in video generation. However, existing token merging [8, 9, 37] applied to the cross-attention have shown suboptimal performance, and applying them to the self-attention in STDiT has observed video quality drops [8, 9].

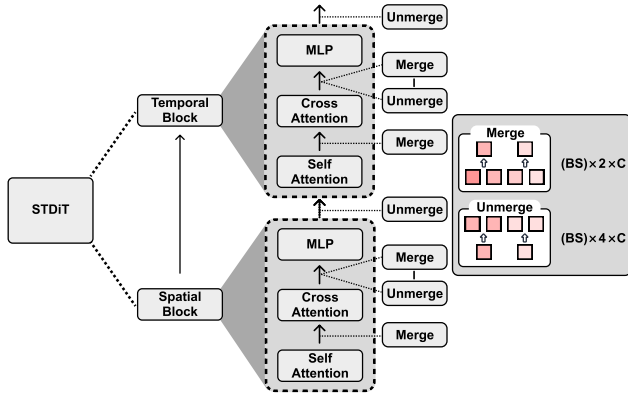


Figure 6: In attention layers of STDiT [82], two consecutive tokens are merged along the temporal dimension and subsequently unmerged after processing, reducing the token size by half and the computational complexity up to a quarter.

### 5.2 Temporal Dimension Token Merging

Figure 6 illustrates Temporal Dimension Token Merging. Based on the hypothesis that successive video frames exhibit similar values, two consecutive frames are merged over the temporal dimension by averaging, creating a single token without an overhead of calculating frame similarity. This reduces the size of tokens by half while preserving the essential temporal information. Consequently, it decreases the computation of self-attention by a factor of four, according to the self-attention’s quadratic complexity,  $\mathcal{O}(n^2)$ . Similarly, it reduces the computation of cross-attention by half, based on the cross-attention’s linear complexity,  $\mathcal{O}(nm)$ . Then, the output token processed through attention modules replicates the dimensions for each frame, restoring them to their original size. Figure 7 depicts the token merging and unmerging.



Figure 7: An illustration of the token merging and unmerging process over the temporal dimension.

Given the token  $T_{in}$  as an input for a self- or cross-attention layer with the dimension  $[B, ST, C]$ , where  $B$  denotes the batch size,  $S$  is the number of pixel patches,  $T$  is the number of frames, and  $C$  is the channel dimension, the input token  $T_{in}$  is merged into  $T_{merged}$ , using the index  $i$ , as:

$$T_{merged} = TDTM_{merge}(T_{in}) \tag{6}$$

$$TDTM_{merge}(T)[i] = \frac{1}{2}(T[:, i, :] + T[:, i + 1, :]) \tag{7}$$

From this, two adjacent tokens are averaged along the temporal dimension, producing the merged token  $T_{merged}$  of  $[B, ST/2, C]$ , which is processed by the self- or cross-attention.

After being processed by each attention,  $T_{merged}$  is unmerged into  $T_{unmerged}$  of the dimension  $[B, ST, C]$  as:

$$T_{unmerged} = TDTM_{unmerge}(Attention(T_{merged})) \tag{8}$$

$$TDTM_{unmerge}(T)[2i] = T[:, i, :] \tag{9}$$

where  $Attention(\cdot)$  is either the self- or cross-attention.

Temporal Dimension Token Merging can be selectively applied during the denoising process to minimize potential negative impacts on video quality that may arise from processing merged tokens. Specifically, out of a total of  $K$  denoising steps, tokens can be merged only for the initial  $k$  steps, while the tokens for the remaining  $K - k$  steps remain unmerged. This is based on the observation that, when tokens are merged along the temporal dimension, the noise values vary slightly across frames—a phenomenon not observed in image diffusion [56] that does not involve a temporal dimension in the generation process. However, because the noise values in the early denoising steps are less subtle and critical, it is expected that applying token merging exclusively for initial steps does not substantially drop video quality.

## 6 Concurrent Inference with Dynamic Loading

We tackle the challenge of limited device memory in text-to-video generation, restricting the on-device inference of large diffusion-based models, by introducing Concurrent Inference with Dynamic Loading (CI-DL), which partitions models and executes them in a concurrent and dynamic manner.

### 6.1 Concurrent Inference

The model components of On-device Sora [41], i.e., STDiT [82] and T5 [52], easily exceed the available memory of many mobile devices, e.g., 3.3 GB RAM of iPhone 15 Pro, as shown in Figure 3. Given that the Transformer architecture [69], which is the backbone for both T5 [52] and STDiT [82], we partition these models into smaller blocks (segments) and load them into memory accordingly for model inference.

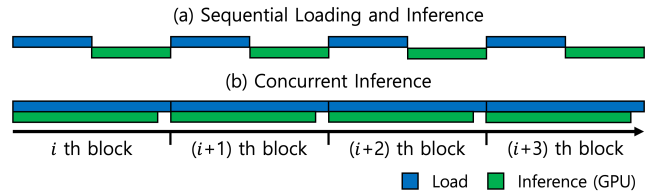


Figure 8: The block loading and inference cycles for (a) sequential loading and inference, and (b) concurrent inference.

To execute model inference using the model partitioning, each block must be loaded sequentially before execution, increasing the overall latency of video generation by incurring block loading time. Figure 8-(a) shows the sequential

block load and inference cycle of STDiT [82], where GPU remains idle intermittently, waiting for each block to be loaded into memory, and only begins execution after the loading is complete. This sequential loading and execution process significantly increases the overall latency of model inference.

To minimize the increase in model inference latency caused by sequential block loading and execution, we propose Concurrent Inference, which leverages both the CPU and GPU for parallel block loading and execution; CPU loads the  $(i + 1)$ th block, while GPU concurrently executes the  $i$ th block. Initially, the first and second blocks are loaded into memory concurrently, with the first block completing its loading first. Subsequently, the inference of the first block and the loading of the second block occur simultaneously. This process continues such that the inference of the  $i$ th block and the loading of the  $(i + 1)$ th block overlap, ensuring continuous parallelism until the final block. Figure 8-(b) depicts the load and inference cycle of STDiT with Concurrent Inference, which shows that GPU is active without almost no idle time by performing block loading and inference in parallel.

Given the number of model blocks  $b$ , block loading latency  $l$ , and inference latency of block  $e$ , the latency reduction  $r$  achieved through Concurrent Inference is given by:

$$r = b \cdot \min(l, e) - \alpha \quad (10)$$

where  $\alpha$  is the overhead caused by the block loading.

Given the large number of denoising steps performed by STDiT, which is partitioned into multiple blocks for execution, similar to T5 [52], the number of blocks  $b$  is expected to be large, leading to a significant reduction in latency. It is expected to accelerate the overall model inference effectively regardless of the device’s memory capacity. When the available memory is limited, then  $b$  increases, while with larger memory, both  $l$  and  $e$  increase. In either case, it can result in an almost constant latency reduction  $r$  in Equation (10).

## 6.2 Dynamic Loading

To further enhance the model inference latency, we propose Dynamic Loading, which is applied in conjunction with Concurrent Inference. It maintains a subset of model blocks in memory without unloading them, with the selection for the subset of blocks to be retained in memory dynamically determined based on the device’s available memory at runtime.

The available memory of the device can vary at runtime based on the system status and configurations of applications running on the mobile device. By retaining a subset of model blocks in memory, the overhead of reloading these blocks during subsequent steps of Concurrent Inference can be eliminated, enabling reductions in model inference latency. To achieve this, we measure the device’s run-time memory capacity and the memory required for inferring a single model block during the initial step of Concurrent

Inference. Next, the memory allocated for retaining certain model blocks is dynamically determined as the difference between the available memory and the memory required for inferring a model block. Then, a series of model blocks that fit within this allocated memory is loaded in a retained state.

Figure 10 depicts Dynamic Loading; the first four model blocks are loaded in a retained state. Unlike other blocks, e.g., the 5th block, these blocks are not unloaded to memory after the initial step, reducing block loading overhead.

Applying Dynamic Loading, the latency reduction  $r$  in Equation (10) for Concurrent Inference is updated as:

$$r = (b - d) \cdot \min(l, e) + d \cdot l - \alpha \cdot (1 - d/b) \quad (11)$$

where  $d$  is the number of blocks maintained in memory. As the number of model blocks retained in memory increases (i.e., a larger  $d$ ), the overhead of loading/unloading blocks is further minimized, fully accelerating the overall model inference under the device’s run-time memory constraints. Dynamically keeping some model blocks in memory with a retained state is particularly advantageous for STDiT [82] that is iteratively executed for denoising steps, which entails loading and reusing the same blocks for each step.

## 7 Implementation

We implement On-device Sora on iPhone 15 Pro [2], leveraging its GPU of 2.15 TFLOPS and 3.3 GB of available memory, with the three methods proposed in Sec. 4, 5, and 6. The model components—T5 [52], STDiT [82], and VAE [17]—in PyTorch [49] are converted to MLPackage, an Apple’s CoreML framework [57] for machine learning apps. Since some state-of-the-art diffusion-related operations required for text-to-video generation are not supported by the current version of CoreML [2], we develop custom solutions, such as xFormer [36] and cache-based acceleration for model inference. Additional implementations, such as denoising scheduling, sampling pipeline, and tensor-to-video conversion, are developed in Swift [3] by utilizing Apple-provided and authenticated libraries. To optimize the models, T5 [52], the largest model used in video generation, is quantized to int8, while other models operated in float32. We found that quantizing STDiT [82] and VAE [17] is challenging due to their sensitivity and performance degradation in video generation. Our future implementations of On-device Sora will explore additional optimization to further enhance model efficiency.

## 8 Experiment

### 8.1 Video Generation Performance

We evaluate the quality of videos generated on an iPhone 15 Pro [2], in comparison to videos produced by Open-Sora [82] running on NVIDIA A6000 GPUs. To assess both temporal and frame-level video quality, we utilize VBench [32],





Figure 9: Example videos generated by On-device Sora and Open-Sora [82] (68 frames, 256×256 resolution).

Table 2: The VBench [32] evaluation by category: On-device Sora vs. Open-Sora [82] (68 frames, 256×256 resolution).

Category	Method	Temporal Quality↑					Frame-Wise Quality↑	
		Subject Consistency	Background Consistency	Temporal Flickering	Motion Smoothness	Dynamic Degree	Aesthetic Quality	Imaging Quality
Animal	Open-Sora	0.97	0.98	0.99	0.99	0.15	0.51	0.56
	On-device Sora	0.95	0.97	0.99	0.99	0.28	0.48	0.55
Architecture	Open-Sora	0.99	0.98	0.99	0.99	0.05	0.53	0.60
	On-device Sora	0.98	0.98	0.99	0.99	0.12	0.49	0.56
Food	Open-Sora	0.97	0.97	0.99	0.99	0.26	0.52	0.60
	On-device Sora	0.95	0.97	0.99	0.99	0.38	0.48	0.53
Human	Open-Sora	0.96	0.97	0.99	0.99	0.38	0.48	0.57
	On-device Sora	0.96	0.96	0.99	0.99	0.43	0.48	0.55
Lifestyle	Open-Sora	0.97	0.97	0.99	0.99	0.23	0.45	0.56
	On-device Sora	0.96	0.97	0.99	0.99	0.25	0.45	0.53
Plant	Open-Sora	0.98	0.98	0.99	0.99	0.15	0.50	0.58
	On-device Sora	0.97	0.98	0.99	0.99	0.16	0.46	0.55
Scenery	Open-Sora	0.98	0.98	0.99	0.99	0.10	0.50	0.50
	On-device Sora	0.97	0.98	0.99	0.99	0.17	0.48	0.47
Vehicles	Open-Sora	0.97	0.97	0.99	0.99	0.37	0.48	0.54
	On-device Sora	0.94	0.96	0.98	0.99	0.44	0.47	0.49

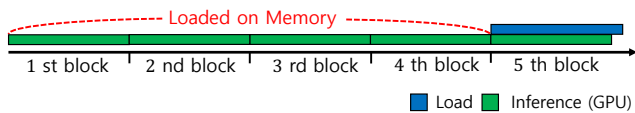


Figure 10: The block loading and inference cycle for Dynamic Loading applied with Concurrent Inference.

the state-of-the-art benchmark for text-to-video generation, which provides a comprehensive evaluation metrics, including subject consistency, background consistency, temporal flickering, motion smoothness, dynamic degree, aesthetic quality, and imaging quality. The evaluation is conducted on 68-frame videos at 256×256 resolution, using text prompts provided by VBench [32], consisting of 100 examples each across eight categories: animals, architecture, food, humans, lifestyle, plants, scenery, and vehicles. Table 2 and Figure 11 present the comparison of the generated videos based on those metrics. The results demonstrate that On-device Sora

generates videos with quality nearly equivalent to Open-Sora in most evaluation metrics, exhibiting only a slight drop in frame-level quality, averaging 0.029, while achieving an average improvement of 0.07 in dynamic degree.

Figure 9 shows example prompts and videos, compared with Open-Sora [82]. For the prompt "a stack of dried leaves burning in a forest", both On-device Sora and Open-Sora generate visually plausible videos, both illustrating stack of burning dry leaves and forest in the background. Similarly, for "close-up of a lemur", both models produce descriptive videos: On-device Sora shows a lemur turning its head, while Open-Sora delivers a less dynamic yet visually comparable depiction.

## 8.2 Linear Proportional Leap

Table 3 presents the video generation performance and speed-up of On-device Sora when applying Linear Proportional Leap (LPL) in Sec. 4. In the table, 'LPL Setting' indicates the

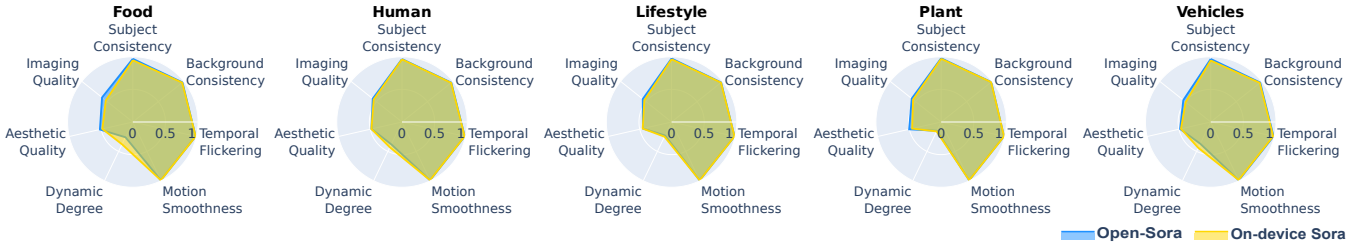


Figure 11: A visual comparison of videos generated by On-device Sora and Open-Sora [82], evaluated using VBench [32].

Table 3: The video quality and generation speedup under different settings of LPL (Linear Proportional Leap).

LPL Setting	SSIM↑	FVD↓	Temporal Quality↑					Frame-Wise Quality↑		Speedup↑
			Subject Consistency	Background Consistency	Temporal Flickering	Motion Smoothness	Dynamic Degree	Aesthetic Quality	Imaging Quality	
16/30 (53%)	0.805	527.27	0.97	0.97	0.99	0.99	0.18	0.50	0.55	1.94×
21/30 (70%)	0.832	344.40	0.97	0.97	0.99	0.99	0.20	0.50	0.56	1.49×
23/30 (76%)	0.840	305.47	0.97	0.97	0.99	0.99	0.21	0.50	0.56	1.34×
25/30 (80%)	0.848	276.68	0.97	0.97	0.99	0.99	0.21	0.50	0.56	1.24×
30/30 (100%)	-	-	0.97	0.97	0.99	0.99	0.21	0.50	0.57	1.00×
Dynamic ( $\mu$ :17.73/30)	0.827	370.86	0.97	0.97	0.99	0.99	0.20	0.50	0.56	1.53×

Table 4: The video quality and speedup under different merging steps of TDTM (Temporal Dimension Token Merging).

Merging Steps	SSIM↑	FVD↓	Temporal Quality↑					Frame-Wise Quality↑		Speedup↑
			Subject Consistency	Background Consistency	Temporal Flickering	Motion Smoothness	Dynamic Degree	Aesthetic Quality	Imaging Quality	
30/30 (100%)	0.595	1225.69	0.97	0.97	0.99	0.99	0.06	0.50	0.56	1.27×
25/30 (83%)	0.599	1168.85	0.97	0.97	0.99	0.99	0.06	0.50	0.56	1.21×
20/30 (66%)	0.604	1056.47	0.97	0.97	0.99	0.99	0.06	0.50	0.56	1.16×
15/30 (50%)	0.612	924.92	0.97	0.97	0.99	0.99	0.12	0.50	0.57	1.13×
10/30 (33%)	0.622	784.67	0.97	0.97	0.99	0.99	0.16	0.50	0.56	1.10×
0/30 (0%)	-	-	0.96	0.97	0.99	0.99	0.23	0.50	0.58	1.00×

number of denoising steps used for video generation out of a total of 30 steps, while the remaining steps are omitted by LPL. We also evaluate a dynamic version of LPL, referred to as ‘Dynamic’ in Table 3, which determines the number of denoising steps at runtime based on the cosine similarities between two adjacent drifts estimated using STDiT [82]. The dynamic LPL stops denoising and makes a proportional leap toward the final video when three cosine similarity measurements fail to improve with tolerance of  $10^{-4}$ , with a minimum 15 denoising steps (50%). Overall, LPL enable the generation of videos whose quality, as measured by SSIM [20], FVD [65], and VBench [32], is comparable to that of Open-Sora [82], without noticeable visual degradation (e.g., 0.740 vs. 0.743 in average of VBench [32]), while accelerating video generation up to 1.94×. It is shown that LPL can reduce denoising latency linearly without incurring computational overhead. By directly reducing denoising steps, it facilitates efficient video generation while maintaining robust performance.

Figure 12 presents example videos generated using LPL, where all LPL settings consistently produce semantically

identical target videos, with most video quality remaining stable across various numbers of denoising steps.

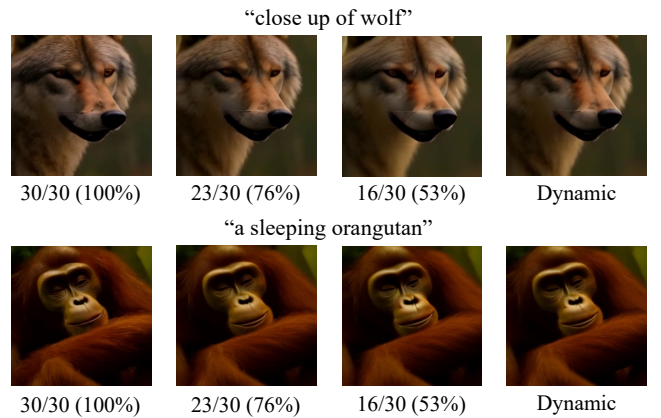
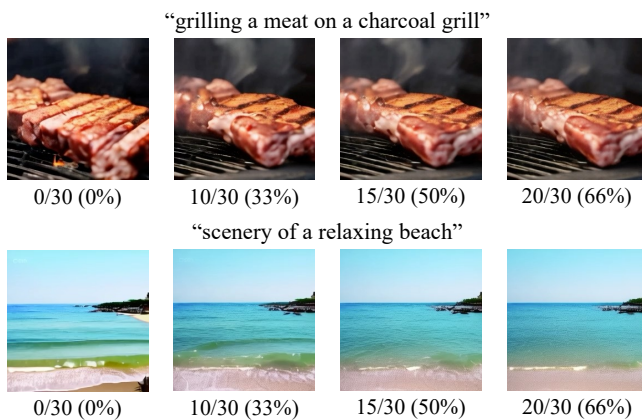


Figure 12: The snapshots of videos (68 frames, 256×256 resolution) applied with various LPL settings (Table 3).

### 8.3 Temporal Dimension Token Merging

Table 4 presents the video quality and video generation speedup achieved when varying numbers of denoising steps to which Temporal Dimension Token Merging (TDTM) (Sec. 5) is applied, indicated as ‘Merging Steps’ in the table, out of a total of 30 denoising steps. Each configuration of merging steps is evaluated on 68-frame videos at a resolution of  $256 \times 256$  pixels, using SSIM [20], FVD [65], and VBench [32] as evaluation metrics. The results indicate that increasing the number of merging steps consistently accelerates video generation, ranging from  $1.10\times$  to  $1.27\times$  speedups, while maintaining stable quality metrics; the average scores for SSIM, FVD, and VBench remain at 0.606, 1032.120, and 0.725, respectively. Nonetheless, declines in the dynamic degree metric is observed, revealing a trade-off between maintaining visual dynamics and reducing token processing complexity. This indicates the importance of striking a balance between video dynamics and speedup. We found that selectively applying TDTM to specific denoising steps can effectively reduce visual noises. For instance, limiting TDTM to the first 15 denoising steps while not applying it to the rest steps tends to result in a less severe quality drop compared to applying TDTM to all steps, which can mitigate issues like flickering or dynamic degree to provide improved video quality.

Figure 13 shows examples of video frames generated with varying numbers of denoising steps to which TDTM is applied, out of 30 steps. The results demonstrate that even as TDTM is applied to an increasing number of denoising steps, the quality of the video frames seems to remain consistent.



**Figure 13: The snapshots of videos (68 frames,  $256 \times 256$  resolution) applied with various merging steps of TDTM (Table 4).**

### 8.4 Concurrent Inference with Dynamic Loading

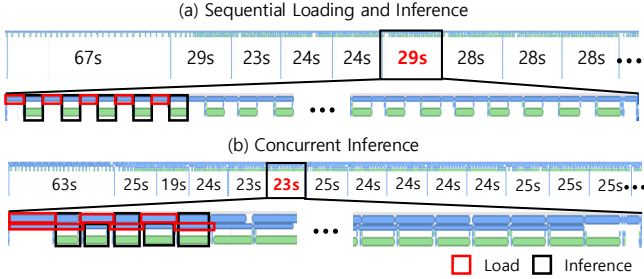
Figure 14-(b) illustrates the model block loading and inference cycles of STDiT [82] when applying the proposed Concurrent Inference (Sec. 6.1), whereas Figure 14-(a) depicts the case without its application. It can be observed that, with Concurrent Inference, the GPU executes each model block for inference without almost no idle time in parallel with the model block loading, indicated by the overlap between the red (loading) and black (inference) boxes in Figure 14-(b), resulting in a block inference latency reduction from 29s to 23s. In contrast, without Concurrent Inference, each model block inference is executed only after the corresponding block is fully loaded to memory, indicated by the lack of overlap between the red (loading) and black (inference) boxes in Figure 14-(a). Consequently, the total latency of the full denoising process using multiple executions of STDiT [82] is reduced by approximately 25%, decreasing from 1,000 to 750 seconds for 30 denoising steps. Given that STDiT is executed multiple times to perform numerous denoising steps, it significantly accelerates the STDiT’s overall inference. In addition, when applied with Dynamic Loading (Sec. 6.2), it achieves an additional average speed improvement of 17 seconds as reloading is not required for certain model blocks that are retained in memory, provided in Equation (11).

Figure 15 shows the case of T5 [52]. Unlike STDiT, which exhibits similar latencies for both block loading and inference execution, T5 exhibits a much longer block loading latency relative to inference latency. Consequently, the overlap between the model loading and inference is minimal, as shown by the small region of overlap between the red (loading) and black (inference) boxes. As a result, the latency improvement is expected to be less substantial, as in Equation (10). Nevertheless, the inference latency is reduced from 164 to an average of 137 seconds, achieving a reduction of 16%. This result implies the effectiveness of concurrent loading and inference, even in cases when there is an imbalance between the latencies of model block loading and inference.

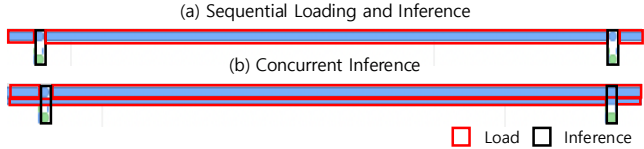
### 8.5 Video Generation Latency

Table 5 shows video generation latencies of two resolutions when each of the proposed methodologies—LPL, TDTM, and CI-DL—is applied individually, as well as the latency when all of them are applied together (‘All’). Latencies are measured with LPL activated at the 15th denoising step and TDTM applied throughout all steps, reported as the mean of three independent experiments. ‘STDiT’ and ‘Total’ specify whether the latency is measured solely for STDiT [82] or for end-to-end video generation, including T5 [52] and VAE [17]. The results demonstrate substantial latency reductions for each methodology compared to the case without





**Figure 14: The block loading and inference cycles of STDiT [82] without (a) and with (b) Concurrent Inference. The red box represents the loading cycle, while the black box indicates the model block inference on the iPhone 15 Pro’s GPU.**



**Figure 15: The block loading and inference cycles of T5 [52] without (a) and with (b) Concurrent Inference.**

using the proposed methods, i.e., 293.51 vs. 1768.32 seconds (Table 1) for STDiT. For the 192×192 resolution video, STDiT (denoising process) takes less than five minutes when all three methodologies are applied. Additionally, it indicates that the methodologies do not interfere with each other, instead work synergistically to enhance latency.

**Table 5: Ablation study on video generation latency (s). ‘All’ denotes the combined application of LPL, TDTM, and CI-DL.**

Resolution	Measurement	LPL	TDTM	CI-DL	All
192×192	STDiT	390.72	696.03	566.81	293.51
	Total	514.24	823.03	691.25	416.50
256×256	STDiT	573.88	965.40	947.67	454.48
	Total	754.08	1148.63	1127.88	638.09

## 9 Discussions and Limitations

**Latency Improvement.** Although On-device Sora enables efficient video generation, the generation latency remains higher compared to utilizing high-end GPUs; it requires several minutes to generate a video, whereas an NVIDIA A6000 GPU takes one minute. This discrepancy is evident due to the substantial disparity in computational resources between them. For instance, the iPhone 15 Pro’s GPU features up to 2.15 TFLOPS with 3.3 GB of available memory, compared to the NVIDIA A6000, which offers up to 309 TFLOPS and 48 GB of memory. Despite this significant resource gap, On-device Sora achieves exceptional efficiency in video generation. Currently, it utilizes only the iPhone 15 Pro’s GPU. We anticipate that the latency could be significantly enhanced if it can leverage NPU (Neural Processing Unit), e.g., the iPhone 15 Pro’s

Neural Engine [2], which delivers a peak performance of 35 TOPS. However, the current limitations in Apple’s software and SDK support for state-of-the-art diffusion-based models [82] make the iPhone’s NPU challenging to utilize effectively. We look forward to the development of software support for NPUs and leave the exploration of this for future work. Also, we plan to investigate the potential of NPUs on a variety of mobile devices, such as Android smartphones.

**Model Optimization.** In On-device Sora, only T5 [52] is quantized to int8, reducing its size from 18 GB to 4.64 GB, while STDiT [82] and VAE [17] are executed with float32 due to their performance susceptibility, which has a significant impact on video quality. Additionally, we do not apply pruning [53] or knowledge distillation [23], as these methods also drop visual fidelity. In particular, we observe that naively shrinking STDiT [82] leads to significant visual loss, caused by iterative denoising steps, where errors propagate and accumulate to the final video. Another practical difficulty in achieving lightweight model optimization is the lack of resources required for model optimization; both re-training and fine-tuning state-of-the-art diffusion-based models typically demand several tens of GPUs, and the available datasets are often limited to effectively apply optimization methods. To tackle this challenge, we propose model training-free acceleration techniques for video generation in this work, i.e., Linear Proportional Leap (Sec. 4) and Temporal Dimension Token Merging (Sec. 5). We recognize further model optimization as a potential direction for our future work.

**Image-to-Video Generation.** Building on the proposed On-device Sora, it is also feasible to extend its capabilities to image-to-video generation, empowering users to create personalized videos based on their own visual data. Furthermore, On-device Sora could evolve to accept both text and images as a multi-modal generative solution, providing an integrated approach to versatile data generation, expected to facilitate the personalization of video generation on mobile devices. We envision that On-device Sora would lay the foundation for future multi-modal visual and textual generation applications on various mobile systems, fostering the on-device revolution and expansion of generative technologies.

## 10 Related Work

**On-device Video Generation.** Numerous video diffusion models have advanced the related technologies, including Make-A-Video [59], Snap Video [44], Imagen Video [27], Video Diffusion [30], Stable Video Diffusion [6], Dreamix [45], MCVD [68], Tune-A-Video [70], Text2Video-Zero [35], among others. Given the substantial resource requirements of video

generation, some studies have investigated optimization under various conditions. For example, QVD [63] employs post-training quantization [42] to enhance computational efficiency and reduce memory usage, while MagicVideo [83] minimizes computations by generating videos in the latent space. CMD [75] decomposes videos into content frames and low-dimensional motion representations to reduce the computational cost of video generation. Similarly, SimDA [71] improves the efficiency of diffusion models by utilizing an effective adapter mechanism. While those studies have sought to enhance the efficiency of video generation, none of them have successfully demonstrated to generate videos on commodity mobile devices, primarily due to high resource demands even after applying their optimization techniques. To the best of our knowledge, the proposed On-device Sora is the first standalone and efficient video generation solution capable of operating on resource-constrained smartphones.

**On-device Image Generation.** There are many works that generate images on the device [4, 10, 33, 38, 66]. However, on-device video generation is struggling due to various challenges. First, video generation requires processing substantially more complex and larger data than image generation [6, 11, 46]. While image generation focuses on a single frame, video generation involves handling multiple frames, with the data requirements scaling with the video’s frame rate (fps) and duration. Additionally, video generation must maintain temporal consistency across frames [44, 59, 71], i.e., it demands maintaining coherent temporal relationships, including object movement, lighting transitions, and background dynamics between successive frames. Achieving this level of consistency necessitates significantly more computation and memory. Furthermore, these requirements often require complex and large models, exacerbating the challenges when operating on resource-limited mobile devices.

**Rectified Flow.** While Open-Sora [82] reduces the number of denoising steps by leveraging Rectified Flow [40], most related approaches [19, 84] require conditioned model training and/or distillation [84]. In contrast, the proposed Linear Proportional Leap effectively reduces the denoising steps without a significant performance drop, as validated using VBench [32], without requiring model re-training or distillation. Notably, it can be easily activated at runtime by just calculating the cosine similarities of drifts between consecutive denoising steps. By developing the current Euler method [12] into more advanced methodologies, it may be possible to further reduce denoising steps while ensuring stability within boundaries. We leave this for future work.

**Token Merging.** Most token merging methods [8, 9, 21] primarily focus on image generation, where tokens are merged based on the spatial similarity rather than temporal similarity. Although some temporal token merging techniques have been proposed, they are applied to models in other

domains [22, 37], not in video generation. As such, Temporal Dimension Token Merging is the first to apply token merging based on the successive similarities between frames in video generation. Additionally, while previous works predominantly apply token merging to self-attention due to performance degradation [8, 9, 21, 37], On-device Sora shows that token merging can be applied to cross-attention with minimal performance loss, achieving 50% merging ratio.

## 11 Conclusion

We propose On-device Sora, the first pioneering solution for generating videos on mobile devices using diffusion-based models, which addresses several key challenges in video generation to enable efficient on-device operation. The issue of extensive denoising steps is addressed through Linear Professional Leap, the challenge of handling large tokens is mitigated with Temporal Dimension Token Merging, and memory limitations are overcome through Concurrent Inference with Dynamic Loading. These proposed efficient on-device video generation methodologies are not limited to On-device Sora but are broadly applicable to various applications, providing significant advancements in on-device video generation without additional model re-training.

## References

- [1] Hervé Abdi. 2007. Singular value decomposition (SVD) and generalized singular value decomposition. *Encyclopedia of measurement and statistics* 907, 912 (2007), 44.
- [2] Apple. 2023. *iPhone 15 Pro—Technical Specifications*. [Online]. Available: <https://support.apple.com/en-us/111829>.
- [3] Apple. 2024. *Swift*. <https://developer.apple.com/swift/>.
- [4] Sergei Belousov. 2021. MobileStyleGAN: A lightweight convolutional neural network for high-fidelity image synthesis. *arXiv preprint arXiv:2104.04767* (2021).
- [5] BN Biswas, Somnath Chatterjee, SP Mukherjee, and Subhradeep Pal. 2013. A discussion on Euler method: A review. *Electronic Journal of Mathematical Analysis and Applications* 1, 2 (2013), 2090–2792.
- [6] Andreas Blattmann, Tim Dockhorn, Sumith Kulal, Daniel Mendelvitich, Maciej Kilian, Dominik Lorenz, Yam Levi, Zion English, Vikram Voleti, Adam Letts, et al. 2023. Stable video diffusion: Scaling latent video diffusion models to large datasets. *arXiv preprint arXiv:2311.15127* (2023).
- [7] Andreas Blattmann, Robin Rombach, Huan Ling, Tim Dockhorn, Seung Wook Kim, Sanja Fidler, and Karsten Kreis. 2023. Align your latents: High-resolution video synthesis with latent diffusion models. In *Proceedings of the IEEE/CVF Conference on Computer Vision and Pattern Recognition*. 22563–22575.
- [8] Daniel Bolya, Cheng-Yang Fu, Xiaoliang Dai, Peizhao Zhang, Christoph Feichtenhofer, and Judy Hoffman. 2022. Token merging: Your vit but faster. *arXiv preprint arXiv:2210.09461* (2022).
- [9] Daniel Bolya, Cheng-Yang Fu, Xiaoliang Dai, Peizhao Zhang, Christoph Feichtenhofer, and Judy Hoffman. 2023. Token Merging: Your ViT But Faster. In *International Conference on Learning Representations*. <https://openreview.net/forum?id=JroZRrW7Eu>
- [10] Thibault Castells, Hyoung-Kyu Song, Tairen Piao, Shinkook Choi, Bo-Kyeong Kim, Hanyoung Yim, Changgwun Lee, Jae Gon Kim, and



- Tae-Ho Kim. 2024. EdgeFusion: On-Device Text-to-Image Generation. *arXiv preprint arXiv:2404.11925* (2024).
- [11] Baoyang Chen, Wenmin Wang, and Jinzhuo Wang. 2017. Video imagination from a single image with transformation generation. In *Proceedings of the on Thematic Workshops of ACM Multimedia 2017*. 358–366.
- [12] Ricky TQ Chen, Yulia Rubanova, Jesse Bettencourt, and David K Duvenaud. 2018. Neural ordinary differential equations. *Advances in neural information processing systems* 31 (2018).
- [13] Yu-Hui Chen, Raman Sarokin, Juhyun Lee, Jiuqiang Tang, Chuo-Ling Chang, Andrei Kulik, and Matthias Grundmann. 2023. Speed is all you need: On-device acceleration of large diffusion models via gpu-aware optimizations. In *Proceedings of the IEEE/CVF Conference on Computer Vision and Pattern Recognition*. 4651–4655.
- [14] Jiwoong Choi, Minkyu Kim, Daehyun Ahn, Taesu Kim, Yulhwa Kim, Dongwon Jo, Hyesung Jeon, Jae-Joon Kim, and Hyungjun Kim. 2023. Squeezing large-scale diffusion models for mobile. *arXiv preprint arXiv:2307.01193* (2023).
- [15] Zijun Deng, Xiangteng He, and Yuxin Peng. 2023. Efficiency-optimized video diffusion models. In *Proceedings of the 31st ACM International Conference on Multimedia*. 7295–7303.
- [16] Prafulla Dhariwal and Alexander Nichol. 2021. Diffusion models beat gans on image synthesis. *Advances in neural information processing systems* 34 (2021), 8780–8794.
- [17] Carl Doersch. 2016. Tutorial on variational autoencoders. *arXiv preprint arXiv:1606.05908* (2016).
- [18] Mohamed Elmasri, Omar Elharrouss, Somaya Al-Maadeed, and Hamid Tairi. 2022. Image generation: A review. *Neural Processing Letters* 54, 5 (2022), 4609–4646.
- [19] Patrick Esser, Sumith Kulal, Andreas Blattmann, Rahim Entezari, Jonas Müller, Harry Saini, Yam Levi, Dominik Lorenz, Axel Sauer, Frederic Boesel, et al. 2024. Scaling rectified flow transformers for high-resolution image synthesis. In *Forty-first International Conference on Machine Learning*.
- [20] Qiang Fan, Wang Luo, Yuan Xia, Guozhi Li, and Daojing He. 2019. Metrics and methods of video quality assessment: a brief review. *Multimedia Tools and Applications* 78 (2019), 31019–31033.
- [21] Zhanzhou Feng and Shiliang Zhang. 2023. Efficient vision transformer via token merger. *IEEE Transactions on Image Processing* (2023).
- [22] Leon Götz, Marcel Kollovich, Stephan Günemann, and Leo Schwinn. 2024. Efficient Time Series Processing for Transformers and State-Space Models through Token Merging. *arXiv preprint arXiv:2405.17951* (2024).
- [23] Jianping Gou, Baosheng Yu, Stephen J Maybank, and Dacheng Tao. 2021. Knowledge distillation: A survey. *International Journal of Computer Vision* 129, 6 (2021), 1789–1819.
- [24] Robert M. Gray and David L. Neuhoff. 1998. Quantization. *IEEE transactions on information theory* 44, 6 (1998), 2325–2383.
- [25] William Harvey, Saeid Naderiparizi, Vaden Masrani, Christian Weibach, and Frank Wood. 2022. Flexible diffusion modeling of long videos. *Advances in Neural Information Processing Systems* 35 (2022), 27953–27965.
- [26] Geoffrey Hinton. 2015. Distilling the Knowledge in a Neural Network. *arXiv preprint arXiv:1503.02531* (2015).
- [27] Jonathan Ho, William Chan, Chitwan Saharia, Jay Whang, Ruiqi Gao, Alexey Gritsenko, Diederik P Kingma, Ben Poole, Mohammad Norouzi, David J Fleet, et al. 2022. Imagen video: High definition video generation with diffusion models. *arXiv preprint arXiv:2210.02303* (2022).
- [28] Jonathan Ho, Ajay Jain, and Pieter Abbeel. 2020. Denoising diffusion probabilistic models. *Advances in neural information processing systems* 33 (2020), 6840–6851.
- [29] Jonathan Ho, Chitwan Saharia, William Chan, David J Fleet, Mohammad Norouzi, and Tim Salimans. 2022. Cascaded diffusion models for high fidelity image generation. *Journal of Machine Learning Research* 23, 47 (2022), 1–33.
- [30] Jonathan Ho, Tim Salimans, Alexey Gritsenko, William Chan, Mohammad Norouzi, and David J Fleet. 2022. Video diffusion models. *Advances in Neural Information Processing Systems* 35 (2022), 8633–8646.
- [31] Zhiting Hu, Zichao Yang, Xiaodan Liang, Ruslan Salakhutdinov, and Eric P Xing. 2017. Toward controlled generation of text. In *International conference on machine learning*. PMLR, 1587–1596.
- [32] Ziqi Huang, Yanan He, Jiashuo Yu, Fan Zhang, Chenyang Si, Yuming Jiang, Yuanhan Zhang, Tianxing Wu, Qingyang Jin, Nattapol Chanpaisit, et al. 2024. Vbench: Comprehensive benchmark suite for video generative models. In *Proceedings of the IEEE/CVF Conference on Computer Vision and Pattern Recognition*. 21807–21818.
- [33] Haolin Jia, Qifei Wang, Omer Tov, Yang Zhao, Fei Deng, Lu Wang, Chuo-Ling Chang, Tingbo Hou, and Matthias Grundmann. 2023. BlazeStyleGAN: A real-time on-device styleGAN. In *Proceedings of the IEEE/CVF Conference on Computer Vision and Pattern Recognition*. 4690–4694.
- [34] Bahjat Kawar, Shiran Zada, Oran Lang, Omer Tov, Huiwen Chang, Tali Dekel, Inbar Mosseri, and Michal Irani. 2023. Imagic: Text-based real image editing with diffusion models. In *Proceedings of the IEEE/CVF Conference on Computer Vision and Pattern Recognition*. 6007–6017.
- [35] Levon Khachatryan, Andranik Movsisyan, Vahram Tadevosyan, Roberto Henschel, Zhangyang Wang, Shant Navasardyan, and Humphrey Shi. 2023. Text2video-zero: Text-to-image diffusion models are zero-shot video generators. In *Proceedings of the IEEE/CVF International Conference on Computer Vision*. 15954–15964.
- [36] Benjamin Lefauveux, Francisco Massa, Diana Liskovich, Wenhan Xiong, Vittorio Caggiano, Sean Naren, Min Xu, Jieru Hu, Marta Tintore, Susan Zhang, Patrick Labatut, Daniel Haziza, Luca Wehrstedt, Jeremy Reizenstein, and Grigory Sizov. 2022. xFormers: A modular and hackable Transformer modelling library. <https://github.com/facebookresearch/xformers>.
- [37] Xirui Li, Chao Ma, Xiaokang Yang, and Ming-Hsuan Yang. 2024. Vid-tome: Video token merging for zero-shot video editing. In *Proceedings of the IEEE/CVF Conference on Computer Vision and Pattern Recognition*. 7486–7495.
- [38] Yanyu Li, Huan Wang, Qing Jin, Ju Hu, Pavlo Chemerys, Yun Fu, Yanzhi Wang, Sergey Tulyakov, and Jian Ren. 2024. Snafusion: Text-to-image diffusion model on mobile devices within two seconds. *Advances in Neural Information Processing Systems* 36 (2024).
- [39] Ming-Yu Liu, Xun Huang, Jiahui Yu, Ting-Chun Wang, and Arun Mallya. 2021. Generative adversarial networks for image and video synthesis: Algorithms and applications. *Proc. IEEE* 109, 5 (2021), 839–862.
- [40] Xingchao Liu, Chengyue Gong, and Qiang Liu. 2022. Flow straight and fast: Learning to generate and transfer data with rectified flow. *arXiv preprint arXiv:2209.03003* (2022).
- [41] Yixin Liu, Kai Zhang, Yuan Li, Zhiling Yan, Chujie Gao, Ruoxi Chen, Zhengqing Yuan, Yue Huang, Hanchi Sun, Jianfeng Gao, et al. 2024. Sora: A review on background, technology, limitations, and opportunities of large vision models. *arXiv preprint arXiv:2402.17177* (2024).
- [42] Zhenhua Liu, Yunhe Wang, Kai Han, Wei Zhang, Siwei Ma, and Wen Gao. 2021. Post-training quantization for vision transformer. *Advances in Neural Information Processing Systems* 34 (2021), 28092–28103.
- [43] Cheng Lu, Yuhao Zhou, Fan Bao, Jianfei Chen, Chongxuan Li, and Jun Zhu. 2022. Dpm-solver++: Fast solver for guided sampling of diffusion probabilistic models. *arXiv preprint arXiv:2211.01095* (2022).
- [44] Willi Menapace, Aliaksandr Siarohin, Ivan Skorokhodov, Ekaterina Deyneka, Tsai-Shien Chen, Anil Kag, Yuwei Fang, Aleksei Stoliar, Elisa Ricci, Jian Ren, et al. 2024. Snap video: Scaled spatiotemporal

- transformers for text-to-video synthesis. In *Proceedings of the IEEE/CVF Conference on Computer Vision and Pattern Recognition*. 7038–7048.
- [45] Eyal Molad, Eliahu Horwitz, Dani Valevski, Alex Rav Acha, Yossi Matias, Yael Pritch, Yaniv Leviathan, and Yedid Hoshen. 2023. Dreamix: Video diffusion models are general video editors. *arXiv preprint arXiv:2302.01329* (2023).
- [46] Kepan Nan, Rui Xie, Penghao Zhou, Tiehan Fan, Zhenheng Yang, Zhijie Chen, Xiang Li, Jian Yang, and Ying Tai. 2024. Openvid-1m: A large-scale high-quality dataset for text-to-video generation. *arXiv preprint arXiv:2407.02371* (2024).
- [47] Zhaoyang Niu, Guoqiang Zhong, and Hui Yu. 2021. A review on the attention mechanism of deep learning. *Neurocomputing* 452 (2021), 48–62.
- [48] Xavier Orriols. 2004. *Generative models for video analysis and 3D range data applications*. Universitat Autònoma de Barcelona.
- [49] Adam Paszke, Sam Gross, Francisco Massa, Adam Lerer, James Bradbury, Gregory Chanan, Trevor Killeen, Zeming Lin, Natalia Gimelshein, Luca Antiga, et al. 2019. Pytorch: An imperative style, high-performance deep learning library. *Advances in neural information processing systems* 32 (2019).
- [50] William Peebles and Saining Xie. 2023. Scalable diffusion models with transformers. In *Proceedings of the IEEE/CVF International Conference on Computer Vision*. 4195–4205.
- [51] Dustin Podell, Zion English, Kyle Lacey, Andreas Blattmann, Tim Dockhorn, Jonas Müller, Joe Penna, and Robin Rombach. 2023. Sdxl: Improving latent diffusion models for high-resolution image synthesis. *arXiv preprint arXiv:2307.01952* (2023).
- [52] Colin Raffel, Noam Shazeer, Adam Roberts, Katherine Lee, Sharan Narang, Michael Matena, Yanqi Zhou, Wei Li, and Peter J Liu. 2020. Exploring the limits of transfer learning with a unified text-to-text transformer. *Journal of machine learning research* 21, 140 (2020), 1–67.
- [53] Russell Reed. 1993. Pruning algorithms—a survey. *IEEE transactions on Neural Networks* 4, 5 (1993), 740–747.
- [54] Robin Rombach, Andreas Blattmann, Dominik Lorenz, Patrick Esser, and Björn Ommer. 2022. High-resolution image synthesis with latent diffusion models. In *Proceedings of the IEEE/CVF conference on computer vision and pattern recognition*. 10684–10695.
- [55] Carl Runge. 1895. Über die numerische Auflösung von Differentialgleichungen. *Math. Ann.* 46, 2 (1895), 167–178.
- [56] Chitwan Saharia, William Chan, Huiwen Chang, Chris Lee, Jonathan Ho, Tim Salimans, David Fleet, and Mohammad Norouzi. 2022. Palette: Image-to-image diffusion models. In *ACM SIGGRAPH 2022 conference proceedings*. 1–10.
- [57] Özgür Sahin and Özgür Sahin. 2021. Introduction to Apple ML tools. *Develop Intelligent iOS Apps with Swift: Understand Texts, Classify Sentiments, and Autodetect Answers in Text Using NLP* (2021), 17–39.
- [58] Tamar Rott Shaham, Tali Dekel, and Tomer Michaeli. 2019. Singan: Learning a generative model from a single natural image. In *Proceedings of the IEEE/CVF international conference on computer vision*. 4570–4580.
- [59] Uriel Singer, Adam Polyak, Thomas Hayes, Xi Yin, Jie An, Songyang Zhang, Qiyuan Hu, Harry Yang, Oron Ashual, Oran Gafni, et al. 2022. Make-a-video: Text-to-video generation without text-video data. *arXiv preprint arXiv:2209.14792* (2022).
- [60] Jiaming Song, Chenlin Meng, and Stefano Ermon. 2020. Denoising diffusion implicit models. *arXiv preprint arXiv:2010.02502* (2020).
- [61] Jianlin Su, Murtadha Ahmed, Yu Lu, Shengfeng Pan, Wen Bo, and Yunfeng Liu. 2024. Roformer: Enhanced transformer with rotary position embedding. *Neurocomputing* 568 (2024), 127063.
- [62] Masahiro Suzuki and Yutaka Matsuo. 2022. A survey of multimodal deep generative models. *Advanced Robotics* 36, 5-6 (2022), 261–278.
- [63] Shilong Tian, Hong Chen, Chengtao Lv, Yu Liu, Jinyang Guo, Xianglong Liu, Shengxi Li, Hao Yang, and Tao Xie. 2024. QVD: Post-training Quantization for Video Diffusion Models. In *Proceedings of the 32nd ACM International Conference on Multimedia*. 10572–10581.
- [64] Thomas Unterthiner, Sjoerd Van Steenkiste, Karol Kurach, Raphaël Marinier, Marcin Michalski, and Sylvain Gelly. 2018. Towards accurate generative models of video: A new metric & challenges. *arXiv preprint arXiv:1812.01717* (2018).
- [65] Thomas Unterthiner, Sjoerd van Steenkiste, Karol Kurach, Raphaël Marinier, Marcin Michalski, and Sylvain Gelly. 2019. FVD: A new metric for video generation. (2019).
- [66] Pavan Kumar Anasosalu Vasu, James Gabriel, Jeff Zhu, Oncel Tuzel, and Anurag Ranjan. 2023. Mobileone: An improved one millisecond mobile backbone. In *Proceedings of the IEEE/CVF conference on computer vision and pattern recognition*. 7907–7917.
- [67] A Vaswani. 2017. Attention is all you need. *Advances in Neural Information Processing Systems* (2017).
- [68] Vikram Voleti, Alexia Jolicoeur-Martineau, and Chris Pal. 2022. Mcvd-masked conditional video diffusion for prediction, generation, and interpolation. *Advances in neural information processing systems* 35 (2022), 23371–23385.
- [69] Thomas Wolf, Lysandre Debut, Victor Sanh, Julien Chaumond, Clement Delangue, Anthony Moi, Pierric Cistac, Tim Rault, Rémi Louf, Morgan Funtowicz, et al. 2020. Transformers: State-of-the-art natural language processing. In *Proceedings of the 2020 conference on empirical methods in natural language processing: system demonstrations*. 38–45.
- [70] Jay Zhangjie Wu, Yixiao Ge, Xintao Wang, Stan Weixian Lei, YuChao Gu, Yufei Shi, Wynne Hsu, Ying Shan, Xiaohu Qie, and Mike Zheng Shou. 2023. Tune-a-video: One-shot tuning of image diffusion models for text-to-video generation. In *Proceedings of the IEEE/CVF International Conference on Computer Vision*. 7623–7633.
- [71] Zhen Xing, Qi Dai, Han Hu, Zuxuan Wu, and Yu-Gang Jiang. 2024. Simda: Simple diffusion adapter for efficient video generation. In *Proceedings of the IEEE/CVF Conference on Computer Vision and Pattern Recognition*. 7827–7839.
- [72] Chenggang Yan, Yunbin Tu, Xingzheng Wang, Yongbing Zhang, Xinhong Hao, Yongdong Zhang, and Qionghai Dai. 2019. STAT: Spatial-temporal attention mechanism for video captioning. *IEEE transactions on multimedia* 22, 1 (2019), 229–241.
- [73] Ling Yang, Zhilong Zhang, Yang Song, Shenda Hong, Runsheng Xu, Yue Zhao, Wentao Zhang, Bin Cui, and Ming-Hsuan Yang. 2023. Diffusion models: A comprehensive survey of methods and applications. *Comput. Surveys* 56, 4 (2023), 1–39.
- [74] Lijun Yu, José Lezama, Nitesh B Gundavarapu, Luca Versari, Kihyuk Sohn, David Minnen, Yong Cheng, Vighnesh Birodkar, Agrim Gupta, Xiuye Gu, et al. 2023. Language Model Beats Diffusion–Tokenizer is Key to Visual Generation. *arXiv preprint arXiv:2310.05737* (2023).
- [75] Sihyun Yu, Weili Nie, De-An Huang, Boyi Li, Jinwoo Shin, and Anima Anandkumar. 2024. Efficient Video Diffusion Models via Content-Frame Motion-Latent Decomposition. *arXiv preprint arXiv:2403.14148* (2024).
- [76] Chenshuang Zhang, Chaoning Zhang, Mengchun Zhang, and In So Kweon. 2023. Text-to-image diffusion models in generative ai: A survey. *arXiv preprint arXiv:2303.07909* (2023).
- [77] Lvmin Zhang, Anyi Rao, and Maneesh Agrawala. 2023. Adding conditional control to text-to-image diffusion models. In *Proceedings of the IEEE/CVF International Conference on Computer Vision*. 3836–3847.
- [78] Xulu Zhang, Xiao-Yong Wei, Wengyu Zhang, Jinlin Wu, Zhaoxiang Zhang, Zhen Lei, and Qing Li. 2024. A Survey on Personalized Content Synthesis with Diffusion Models. *arXiv preprint arXiv:2405.05538* (2024).

- [79] Wayne Xin Zhao, Kun Zhou, Junyi Li, Tianyi Tang, Xiaolei Wang, Yupeng Hou, Yingqian Min, Beichen Zhang, Junjie Zhang, Zican Dong, et al. 2023. A survey of large language models. *arXiv preprint arXiv:2303.18223* (2023).
- [80] Yang Zhao, Yanwu Xu, Zhisheng Xiao, and Tingbo Hou. 2023. Mobilediffusion: Subsecond text-to-image generation on mobile devices. *arXiv preprint arXiv:2311.16567* (2023).
- [81] Kaiwen Zheng, Cheng Lu, Jianfei Chen, and Jun Zhu. 2023. Dpm-solver-v3: Improved diffusion ode solver with empirical model statistics. *Advances in Neural Information Processing Systems* 36 (2023), 55502–55542.
- [82] Zangwei Zheng, Xiangyu Peng, Tianji Yang, Chenhui Shen, Shenggui Li, Hongxin Liu, Yukun Zhou, Tianyi Li, and Yang You. 2024. *OpenSora: Democratizing Efficient Video Production for All*. <https://github.com/hpcaitech/Open-Sora>
- [83] Daquan Zhou, Weimin Wang, Hanshu Yan, Weiwei Lv, Yizhe Zhu, and Jiashi Feng. 2022. Magicvideo: Efficient video generation with latent diffusion models. *arXiv preprint arXiv:2211.11018* (2022).
- [84] Yuanzhi Zhu, Xingchao Liu, and Qiang Liu. 2025. SlimFlow: Training Smaller One-Step Diffusion Models with Rectified Flow. In *European Conference on Computer Vision*. Springer, 342–359.